HHS Public Access

Author manuscript

Mucosal Immunol. Author manuscript; available in PMC 2016 May 18.

Published in final edited form as:

Mucosal Immunol. 2016 January ; 9(1): 68–82. doi:10.1038/mi.2015.36.

High-dimensional immune profiling of total and rotavirus VP6-specific intestinal and circulating B cells by mass cytometry

Nitya Nair[1,7], **Evan W. Newell**[2,7], **Christopher Vollmers**[3], **Stephen R. Quake**[3], **John M. Morton**[4], **Mark M. Davis**[5,6,7], **Xiao-Song He**[1,7], and **Harry B. Greenberg**[1,7,*]

[1]Department of Medicine, Stanford University, Stanford, CA 94305, USA

[2]Agency for Science, Technology and Research (A*STAR), Singapore Immunology Network (SIgN), Singapore

[3]Department of Bioengineering, Stanford University, Stanford CA 94305, USA

[4]Department of Surgery, Stanford University School of Medicine, Stanford CA 94305, USA

[5]The Howard Hughes Medical Institute, Stanford, CA 94305, USA

[6]Institute for Immunity, Transplantation and Infection, Stanford University, Stanford CA 94305, USA

[7]Department of Microbiology and Immunology, Stanford University, Stanford, CA 94305, USA

Abstract

In-depth phenotyping of human intestinal antibody secreting cells (ASCs) and their precursors is important for developing improved mucosal vaccines. We used single-cell mass cytometry to simultaneously analyze 34 differentiation and trafficking markers on intestinal and circulating B cells. In addition, we labeled rotavirus double-layered particles with a metal isotope and characterized B cells specific to the rotavirus VP6 major structural protein. We describe the heterogeneity of the intestinal B cell compartment, dominated by ASCs with some phenotypic and transcriptional characteristics of long-lived plasma cells. Using principal component analysis, we visualized the phenotypic relationships between major B cell subsets in the intestine and blood, and revealed that IgM^+ memory B cells (MBCs) and naïve B cells were phenotypically related as were $CD27^-$ MBCs and switched MBCs. ASCs in the intestine and blood were highly clonally related, but associated with distinct trajectories of phenotypic development. VP6-specific B cells were present among diverse B cell subsets in immune donors, including naïve B cells, with phenotypes representative of the overall B cell pool. These data provide a high dimensional view of intestinal B cells and the determinants regulating humoral memory to a ubiquitous, mucosal pathogen at steady-state.

*Corresponding author, ; Email: hbgreen@stanford.edu

Conflict of interest

The authors have no conflict of interest to report.

DISCLOSURE

The authors have no conflict of interest to report.

Keywords

Human intestinal B cells; mass cytometry; rotavirus

INTRODUCTION

Diarrheal diseases are a leading cause of morbidity and mortality in infants less than 5 years of age in developing countries[1]. Protective immunity against many intestinal pathogens is mediated by local antibody secreting cells (ASCs) through the production of secretory antibodies (Abs)[2]. Since several oral vaccines that mediate protection via local induction of Abs are less effective in developing countries[3], in-depth phenotypic characterization of intestinal ASCs, and their precursors, in healthy donors is an important initial step for the development of improved vaccines.

Among the causative agents of diarrheal disease, rotaviruses (RV) are the leading cause of severe pediatric gastroenteritis worldwide[4]. Two safe and effective oral RV vaccines have been licensed, however the immunologic basis for the efficacy of these vaccines is unknown. Neutralizing antibodies to RV target the two viral surface proteins, VP4 and VP7. In addition, the major capsid protein, VP6, elicits a dominant Ab response post infection. VP6-specific Abs do not neutralize RV *in vitro* but some can inhibit RV replication intracellularly[5] and prevent or resolve RV infection in a mouse model[6]. Furthermore, single chain VP6-specific Abs exhibit neutralizing activity *in vitro* and can confer protection against RV-induced diarrhea *in vivo*[7].

The role of VP6 Abs in mediating protection in humans is not known. In peripheral blood VP6-binding reactivity is detected at steady state in healthy donors in switched memory B cells (MBCs), IgM^+ MBCs, $CD27^-$ MBCs and naïve B cells[8–10]. The interaction of VP6 with surface Ig on naïve B cells has been reported in adult and cord blood at a frequency of ~2% of naïve B cells[9]. VP6-specific naïve B cells exhibit distinct VH1-46 immunoglobulin gene segment bias in infant and adult repertoires[11, 12], while somatic mutations of non-dominant clones is characteristic of the VP6-specific MBC repertoire[10]. IgM^+ MBCs specific to VP6 are capable of switching to IgG *in vitro* and *in vivo* and mediate antiviral effects *in vivo*[13]. VP6-specific intestinal plasma cells have also been detected at steady state in healthy adult donors and have been used to generate monoclonal Abs[14], however, comprehensive phenotypic characterization of VP6-specific intestinal B cells has not been reported.

Mass cytometry (CyTOF) is an advanced technology in multi-dimensional analysis of protein expression that facilitates multiparametric immune phenotyping of individual cells. The mass cytometry platform relies on the use of antibodies tagged with stable metal isotopes that are used to stain cells, which in turn are analyzed by a time of flight (TOF) mass spectrometer[15, 16]. The use of metal isotope-tagged antibodies circumvents problems of spectral overlap inherent in fluorescence-based cytometry, and offers an increase in the number of measurable parameters (~40) per individual cell, while obviating the need to perform compensation across channels[15, 16]. Multiparametric phenotypic measurements at single cell resolution facilitate high dimensional analysis and visualization of relationships

between lymphocyte subsets in continuous development[17, 18] rather than as a static characterization of the overall cellular pool, as has been reported for signaling in human hematopoiesis[15], CD8 T cell diversity[19–21] and B cell lymphopoieisis[22].

We used mass cytometry for high dimensional phenotypic analysis of the human small intestinal B cell compartment by simultaneously measuring the expression of 34 markers specific for B cell differentiation and mucosal trafficking on individual B cells in the intestine and blood of healthy adults. Using principal component analysis (PCA) to analyze high dimensional mass cytometry data, we visualized the phenotypic relationships between major B cell subsets, and revealed that IgM^+ memory B cells (MBCs) and naïve B cells were phenotypically closely related as were $CD27^-$ MBCs and switched MBCs. We demonstrate that intestinal and circulating ASCs are highly clonally related in terms of Ab repertoires, despite distinct trajectories of phenotypic development. In addition, we characterized some phenotypic and transcriptional features of intestinal ASCs implicated in longevity, including HLA-$DR^{+/-}CD95^-$ expression and the upregulation of *Bcl-2*, *Blimp-1* and *XBP-1*. Finally, we generated metal isotope-labeled RV double-layered particles (DLPs) and validated their use in the identification of VP6-specific B cells by mass cytometry. We demonstrate broad VP6-binding reactivity across both intestinal and circulatory ASCs and other B cell subsets in RV immune adults at steady-state, with phenotypes representative of the overall B cell pool. This work provides novel resolution and insight into the phenotypic complexity of human intestinal B cells and to the mechanisms regulating humoral memory to an important mucosal pathogen at steady-state.

RESULTS

Combinatorial expression of mucosal trafficking markers in ASCs and other B cell subsets in the intestine and blood at steady state

B cells isolated from proximal jejunum resections from adult gastric bypass patients and peripheral blood from the same patients (n=7) were used for immune phenotyping by mass cytometry. In addition, intestinal resections were obtained without simultaneous blood samples (n=3) or blood samples were obtained from a blood bank (n=10). Boolean gating was used to identify intestinal mature B cells as $CD3/14/16/56^-$ $CD19^+$ or $CD27^{hi}CD38^{hi}$ [23]. Peripheral blood B cells were identified as $CD19^+$. ASCs and non-ASC B cell subsets (switched memory B cells (MBC), $CD27^-$ MBCs, IgM^+ MBCs and naïve B cells) were identified in the intestine and the blood of all donors (Fig. 1A, Fig. S1–S3). Spanning-tree progression analysis of density-normalized events (SPADE) [24] was used to simultaneously measure the expression of mucosal trafficking markers on intestinal and circulating B cells. Nodes of phenotypically similar cell clusters corresponding to ASCs and non-ASC B cell subsets were identified based on the expression of B cell lineage markers in all seven donors analyzed (Fig. 1B, Fig. S5) and were used to analyze quantitative and qualitative differences between subsets[15, 24, 25]. In all donors analyzed, intestinal ASCs were $CCR6^{lo/-}CCR7^{lo/-}$ $CCR10^+Int\beta1^+CXCR4^+Alpha4^{lo}Int\beta7^{lo/-}$; in contrast, circulating ASCs were $CCR6^{lo/-}$ $CCR7^{+/-}CCR10^{+/-}Int\beta1^+CXCR4^+Alpha4^{hi}Int\beta7^+$ (Fig. 1C, Fig. S5). With the exception of naïve B cells, all intestinal B cells expressed at least 3-fold higher levels of CXCR4 than circulating B cells (ASC, P=0.002; switched MBC, P<0.0001; IgM^+ MBC, P=0.0004).

Circulating ASCs expressed higher levels of Alpha4 and Intβ7 than intestinal ASCs ($P<0.05$). Analysis of the simultaneous expression of six mucosal trafficking markers in individual nodes of all the seven donors revealed a combinatorial diversity of phenotypes (Fig. 2).

Intestinal ASCs exhibit phenotypic and transcriptional characteristics of long-lived plasma cells

Some of the phenotypic and transcriptional characteristics of intestinal ASCs ($CD20^{lo/-}$ $CD27^{hi}$ $CD38^{hi}$), implicated in longevity, were determined. Intestinal and circulating ASCs expressed lower levels of surface IgA and CD40 than switched MBCs, whereas intestinal ASCs expressed higher levels of CCR10 and CD138 compared to circulating ASCs (Fig. 3A). In contrast to circulating ASCs that are HLA-$DR^{+/-}CD95^{+}$, intestinal ASC are HLA-$DR^{-}CD95^{-}$ suggesting non-responsiveness to apoptosis via CD95 ligation (Fig. 3A, B, C). Among the circulating ASCs that were HLA-DR^{-}, some expressed CD138 and all were $CD95^{+}$ (Fig. 3B). Based on quantitative RT-PCR analysis of sorted intestinal ASCs and MBCs (Fig. S4, Table S2), the mRNA encoding anti-apoptotic transcription factor Bcl-2 was expressed at higher levels in intestinal ASCs than in intestinal MBCs ($P=0.048$), as were *Blimp-1* ($P=0.038$) and *XBP-1* ($P=0.009$), upregulated during plasma cell differentiation[26] (Fig. 3D, Table S2). *Bcl-6*, required for germinal center formation, was expressed by intestinal MBCs but not by intestinal ASCs ($P=0.013$). IgA secretion was detected from sorted intestinal ASCs at steady-state (median frequency (range), 2.92×10^5 per 10^6 B cells ($1.98 \times 10^5 – 4.58 \times 10^5$)) and for up to 5 days *in vitro* in the presence of CpG-2006 and IL-2 (9.90×10^4 per 10^6 B cells ($1.79 \times 10^4 – 1.80 \times 10^5$)) (Fig. S3C, D, E, Fig. S4, Table S2). Based on these measured parameters, these data suggest that intestinal ASCs share some phenotypic and transcriptional attributes with quiescent, terminally differentiated, long-lived bone marrow plasma cells[27] but are unlike pro-apoptotic plasmablasts in circulation or tonsil-derived plasma cells[28]. Analysis of additional transcriptional and functional features of intestinal and bone marrow ASCs in the same individuals will be required to further explore these findings.

Dimensionality reduction by PCA reveals phenotypic relationships between B cell subsets in the intestine and blood

Principal component analysis (PCA) was used to visualize the high dimensional mass cytometry datasets[17, 18, 29]. PCA defines components that cumulatively account for the variation contained within the entire dataset, with the first three components in this analysis accounting for most of the total variation. PCA allows the patterns of expression of all 34 markers to be summarized for each cell, which can then be viewed on a 2D or 3D plot, thereby allowing different cell populations to be viewed in relation to one another[18, 21, 29].

Since the phenotypes of ASCs and non-ASCs were so different, PCA was more informative when they were analyzed separately (Fig. 4A, B, Fig. S6A, B). Visualization of the first two principal components of ASCs (Fig. 4B, Fig. S6B) and non-ASCs (Fig. 4A, Fig. S6A) provided an overview of the phenotypic complexity of intestinal and circulating B cells. The general arrangement of clusters was conserved across the seven donors analyzed (Fig. 4A, B). Non-ASC subsets were identified by manual gating (Fig. S3A), overlaid on 2D plots and

used to identify the composition of the clusters (Fig. 4A, Fig. S6A) as previously described[19–21]. In the blood, IgM^+ MBCs and naïve B cells were phenotypically related and distinct from $CD27^-$ MBCs and switched MBCs. $CD27^-$ and switched MBCs were phenotypically more related to each other than to the IgM^+ MBCs and naïve B cells. This trend was also observed in the intestinal data; however in some donors IgM^+ MBCs also overlapped with switched MBCs, suggesting greater complexity of IgM^+ MBCs in the intestinal milieu compared to the blood. ASCs, switched MBCs, and $CD27^-$ MBCs were gated based on isotype expression and IgA^+, IgM^+, and IgG^+ cells within each subset were identified (Fig. 4C, D). IgG^+ ASCs were phenotypically more distinct from IgA^+ ASCs than were IgM^+ ASCs. The amount of variance described by each principle component was quantified to estimate the cumulative effectiveness of each analysis. The first two principal components cumulatively accounted for 45% (27–50%) of the variation in the entire dataset (Fig. 4E, F, Fig. S6E). The addition of the third principal component increased the cumulative variation coverage to 50% (35–56%). Any single additional principal component, beyond the first three components, did not contribute to significantly more variation and thus were not included in analyses. Loading values, or weighting coefficients, provided insight on the contribution of each marker to the first two principal components (Fig. 4G, H, Fig. S6F, G). This same analysis was run on each donor independently; the general features of the analysis were preserved on independent repeats among different donors analyzed (Figure S6A, B).

Visualization of the first three principal components revealed an ordered arrangement of non-ASC B cell subsets that recapitulated the trajectory of B cell differentiation. Naïve B cells and IgM^+ MBCs were phenotypically closely related. $CD27^-$ MBCs were observed as a transitional population between IgM^+ MBCs and switched MBCs; this separation was more evident in the blood than in the intestine. Switched MBCs occupied a phenotypic niche distinct from the other non-ASC subsets (Fig. 5A, Movie S1A, B). A multitude of unique, transitional cell states were observed between the major B cell subsets in the intestine and the blood.

3D PCA was used to directly compare the phenotypic relationships between intestinal and circulating ASCs and non-ASC B cells. ASCs in the intestine and blood were phenotypically distinct (Fig. 5B). Non-ASCs in the intestine and blood partially clustered together but also exhibited some distinct, compartment-specific clusters (Fig. 5C). To determine which specific non-ASC subsets were phenotypically related in the intestine and blood, each B cell subset in the blood and intestine was plotted on an individual 3D plot. This analysis revealed that naïve B cells are closely related in the intestine and the blood. With progressive B cell differentiation, phenotypic relatedness decreased among non-ASC subsets in the intestine compared to the blood. Switched MBCs and ASCs occupied almost entirely distinct phenotypic niches in the two compartments (Fig. 5D).

Total intestinal and circulating ASCs are clonally related as revealed by Ab repertoire lineage analysis

Having compared the phenotypes of intestinal and circulating B cells we then directly compared intestinal and circulating Ab lineages using a sequencing approach that

incorporates unique barcode labels on the same Ab heavy chain (IGH) RNA molecule[30]. These labels permit multiple sequencing reads derived from the same RNA molecule after extensive amplification to be combined so as to reduce the sequencing error rate and enable accurate quantification of RNA and isotype. IGH lineages were defined as sequences with identical V and J segment usage and ≥90% identity in junction regions, thus originating from the same B cell clone.

Total circulating ASCs and naïve B cells were sorted to ≥96% purity from PBMCs obtained from two donors and IGH lineages shared between sorted ASCs or naïve B cells and the unsorted PBMCs facilitated identification of subset-specific IGH lineages among the total PBMCs based on IGH transcript abundance, mutation and isotype (Fig. 6A). Total ASCs expressed highly abundant, mutated class-switched IGH lineages while total naïve B cells expressed low abundance, non-mutated IgM lineages. These trends were consistent between the two subjects analyzed and were used to identify total ASC and naïve B cell lineages among total B cells in the intestine and the blood of the same donor (Fig. 6B). The peripheral blood Ab repertoire was dominated by IgA and naive IgM lineages (Fig. 6C). IgA lineages were highly abundant and therefore ASC-derived. Non-mutated IgM lineages were low in abundance and therefore derived from naive B cells (Fig. 6D,E). The intestinal Ab repertoire was dominated by IgA lineages (Fig. 6C), but was largely devoid of naive, low-abundance IgM lineages (Fig. 6D,E), consistent with mass cytometry data (Fig. S3B) and previous studies[2, 31].

To determine the direct clonal relationships between total intestinal and circulating B cells, we compared the percentage of shared Ab lineages between the two compartments. Of note, there were 1053 highly abundant IgA lineages in circulating B cells; of these, 385 were also detected in intestinal B cells. The 36.5% of shared sequences was higher than the extent of shared lineages between peripheral blood samples obtained at the same time from the same individual (~25%)[30], suggesting that the intestinal and circulating IgA^+ ASCs are highly related (Fig. 6B). Lineages were also shared among IgG^+ (25.5%) and IgM^+ (23.2%) ASCs in the intestine and the blood. Among non-ASCs, lineages were shared in IgA repertoires (11.6%) and few lineages were shared among IgG (4.1%) or IgM (1.5%) repertoires.

Major intestinal and circulating B cell subsets demonstrate VP6 reactivity at steady state

The mass cytometry platform was then applied to the identification RV VP6-specific B cells. Rhesus rotavirus (RRV) DLPs that possess an inner capsid composed of VP6 and VP2 but lack an outer capsid containing VP4 and VP7, were labeled with erbium 166 (Er166) and used to stain B cells expressing VP6-specific Ig. Since metal-labeled antigens have not been used to identify antigen-specific B cells previously, the specificity and sensitivity of this approach was verified with BCR staining and blocking experiments in mice and humans. It is virtually impossible to obtain a RV-naïve adult that could be used to verify DLP-specific B cell staining. Therefore, we first demonstrated that DLP-Er166 stained VP6-specific but not VP4-specific murine hybridoma cells. Blocking with unlabeled DLPs reduced DLP-Er166-specific staining on VP6-specific hybridomas (Fig. 7A). Next we stained human peripheral blood B cells with DLP-Er166 in the presence and absence of unlabeled DLPs. Unstained control samples were used to identify VP6-specific B cells. Blocking reduced DLP-Er166

staining on total B cells by 90% (0.45% to 0.05% of $CD19^+$ B cells) (Fig. 7B). In peripheral blood samples, DLP-Er166-binding cells were present among switched MBCs, IgM^+ MBCs, $CD27^-$ MBCs, and naïve B cells (Fig. 7C, Fig. S7A), consistent with previous flow cytometry studies using VLP-VP2-GFP/VP6[8–10]. Lastly, blocking with unlabeled DLPs reduced DLP-Er166 binding to B cells in all B cell subsets by ≥8-fold (switched MBCs 0.28% to 0.04%; IgM^+ MBCs 0.55% to 0.04%; $CD27^-$ MBCs 0.53% to 0.07%; naïve B cells 0.40% to 0.05%) ($P<0.0001$)(Fig. 7C, Fig. S7A). The frequencies of VP6-specific B cells among total B cells (Fig. S7B) and among switched MBCs, IgM^+ MBCs, $CD27^-$ MBCs and naïve B cells (Fig. S7C) were comparable using the mass cytometry and flow cytometry platforms. In parallel work in our laboratory, we labeled DLPs with Cy5 and used this conjugate to single-cell sort intestinal IgA^+ ASCs into RNA lysis buffer for RT-PCR amplification of Ig variable genes and mAb expression (Fig. S7D, E, F). Seven of the nine expressed mAbs bound DLPs, as determined by Elisa, further demonstrating specificity of the VP6-specific B cell staining. Analysis of V gene segment usage among VP6-sepcific intestinal IgA^+ ASCs revealed an over representation of the VH4 gene family, consistent with previous work by Di Niro et al[14].

VP6-specific intestinal and circulating B cells from the same healthy, adult donors were characterized by mass cytometry. VP6-specific intestinal B cells were detected among ASCs, switched MBCs, IgM^+ MBCs, $CD27^-$ MBCs and naïve B cells (Fig. 7D, E, F, Fig. S7B). This reactivity among diverse subsets was also observed in circulating B cells from the same donors: DLP-Er166 binding reactivity was observed to switched MBCs, IgM^+ MBCs, $CD27^-$ MBCs and naïve B cells, consistent with previous studies[8–10]. VP6-specific ASCs were present at a median frequency of 0.5% (0–0.1%) of total ASCs in the intestine and were not detected in the blood in the seven donors analyzed. The median frequency of VP6-specific switched MBCs was higher in the intestine [2.1% (0.3–3.0%)] compared to the blood [0.3% (0–2.8%)]($P=0.007$)(Fig. 7E). In contrast, the median frequencies of VP6-binding IgM^+ MBCs, $CD27^-$ MBCs and naïve B cells in the intestine and blood were not significantly different ($P=0.09$, $P=0.29$, $P=0.39$). The phenotypes of VP6-specific B cells, compared to VP6-non-specific B cells, did not differ in ASCs or other B cell subsets in the intestine or in the blood, as determined by clustered heatmap analysis of 34 cell surface markers (Fig. 7G).

DISCUSSION

In this study we provide a high dimensional view of the phenotypic heterogeneity of human intestinal B cells, and use PCA to visualize the phenotypic relationships between ASCs and other B cell subsets in the intestine compared to the blood. Human intestinal B cells have been extensively characterized by flow cytometry and immunohistochemistry[31–34]. Since the mass cytometry platform facilitates the analysis of many more parameters per individual cell while circumventing problems of spectral overlap, we extend these fluorescence-based analyses to reveal phenotypic complexity at a systems level and a heterogeneity far greater than previously appreciated. These initial data lay the foundation for future studies to determine the microanatomical derivation of ASCs and non-ASC subsets within the intestinal mucosa as well as their functional contribution.

One of the major advances of this work is the validation of the mass cytometry platform for the identification of antigen-specific B cells, as demonstrated in the analysis of RV VP6-specific B cells. Virtually all adults have been infected with RV on several occasions and have established humoral memory that generally protects from repeat disease. Thus current RV vaccines do not generally induce detectable immune responses in adults since all adults are immune to these live viral vaccines due to prior exposure, in many cases multiple exposures. Since RV is a ubiquitous pathogen, persistent exposure and subclinical infection likely result in the re-stimulation of RV-reactive MBCs to ASCs in the intestinal mucosa. Murine studies have also demonstrated persistence of RV-specific ASCs in the mouse intestine after a single RV infection[35]. We report the breadth of B cell subsets with reactivity to VP6 that constitute part of this memory response in RV-infection experienced adults and frequencies of VP6 specific ASCs and switched MBCs that were significantly higher in the intestine (ASCs 0.5% vs 0%; switched MBCs 2.1% vs 0.3%), the primary site of RV infection, than in circulation. Although VP6-specific Abs will not block RV entry into epithelial cells, they may restrict viral replication[5, 6]. This steady-state Ab response to a ubiquitous pathogen may represent a mechanism through which humoral memory to RV is maintained. It should be noted that most IgA^+ and IgM^+ ASCs maintain surface Ig expression. However, identification of IgG^+ ASCs based on surface Ig expression is limited to a subset of cells that express surface Ig, as many IgG^+ ASCs have downregulated expression of cell surface B cell receptor (BCR)[23, 36].

The functions of ASCs, switched MBCs, and IgM^+ MBCs in mediating humoral immunity to RV have been studied[13], however the roles of $CD27^-$ MBCs and naïve B cells remain unclear. Naïve B cells specific to VP6 have been reported in circulation in healthy adults at steady state[8, 9] and could represent an innate repertoire comprised of natural Abs due to optimal VP6-interacting germline-encoded surface Ig, or may result from an early T-independent B cell response to RV. Innate-like intestinal B cells capable of iNos and TNF-α secretion have been described in the mouse lamina propria[37]. Ab repertoire studies showed that usage of VH1-69 was higher in the VP6-specific naïve B cell repertoire compared to total naïve B cells in circulation[10]. This gene segment encodes a hydrophobic CDR-H2 and has been implicated in early viral responses and polyspecificity[38].

The observation that multiple B cell subsets have reactivity to VP6 at steady state contrasts the B cell response to tetanus toxoid[39] or to VP7[9], for which reactivity is present solely among switched MBCs. The broad VP6-binding reactivity may represent a regulated mucosal response to a non-neutralizing epitope present on a ubiquitous pathogen. During RV replication and cell lysis, a large amount of extracellular VP6 is exposed to the immune system. Regulating the class-switched, high-affinity response toward neutralizing epitopes present on VP4 and VP7, while directing some class-switched MBCs and but predominantly low affinity, IgM responses to VP6[13, 40], may be advantageous as IgG and IgA responses have been associated with intestinal inflammation[41, 42]. Further studies are required to assess the functional contribution of VP6-specific B cells in mediating immunity to RV. Since metal labeling of antigens is applicable to a range of proteins, these tools may aid in the improved understanding of the complexity of B cells induced by a variety of infections and vaccinations[16].

Little is known regarding the migration and lifespan of intestinal ASCs. Several observations have suggested that mucosal plasma cells are short-lived[43]; however, plasma cells from small intestine biopsies secrete IgA *in vitro* for up to 4 weeks[44] and colonic and bone marrow plasma cells express Bcl-2, are $CD95^{+/lo}$ and non-responsive to CD95 ligation *in vitro*[34]. In contrast, circulating and tonsillar ASCs are $CD95^{hi}$ and can be driven to apoptosis *in vitro* via CD95 ligation[28]. Here we demonstrated that, based on some phenotypic and transcriptional parameters, intestinal ASCs were similar to quiescent, terminally differentiated, long-lived bone marrow plasma cells ($HLADR^{-}$ $CD95^{lo/-}CD40^{-}CD180^{-}CD138^{+/-}$ phenotype and higher expression levels of *Bcl-2*, *Blimp-1, IRF-4* and *XBP-1* compared to intestinal MBCs). However, direct comparisons between intestinal and bone marrow ASCs in the same individuals, and measurement of the expression of *Ki67, BCMA* and *Mcl1* will be required to fully explore these initial findings. We detected persistent IgA secretion by intestinal ASCs for up to 5 days *in vitro* in the presence of CpG-2006 and IL-2. The downregulation of CD95 was unique to intestinal ASCs, as all circulating ASCs, including the few that were $HLA^{-}DR^{-}CD138^{+/-}$, expressed high levels of CD95. CXCL12, the ligand for CXCR4, is important for the survival of bone marrow plasma cells[45] and for plasmablast homing to the bone marrow[46]. We observed higher expression of CXCR4 on intestinal ASCs compared to circulating ASCs, however whether or not mucosal tissue provides survival niches for long-lived plasma cells remains unclear[47]. Analysis of proliferation markers, such as Ki67, and the expression of *Mcl1*[48], associated with antiapoptotic pathways in plasma cells, will be required to extend these initial observations. Interestingly, we detected expression of *Bcl-6* in intestinal MBCs. Bcl-6 expression is associated with GC B cells[49], however, GC B cells were excluded from this analysis since we identified intestinal MBCs based on $CD20^{+}$ $CD27^{+}$ $CD38^{int/-}$ phenotype and sorted these cells to >99% purity. Furthermore, we verified that the intestinal MBCs secreted IgA following a 5 day *in vitro* stimulation with CpG-2006 and IL-2. Of note, the expression of CCR9 has been implicated as an important trafficking marker to the human small intestine, however due to lack of suitable staining with available Ab clones we were unable to stain for this marker. However circulating ASCs expressed the gut trafficking markers, Alpha4 and Intβ7, that were downregulated in intestinal ASCs. Intestinal ASCs expressed Intβ1 and CXCR4, factors implicated in ASC trafficking to the upper aerodigestive epithelium and bone marrow respectively[50], suggesting a promiscuous homing capacity for these cells.

Clonal relationships between IgG^{+} B cells in the colon and blood[51], and between colonic B cells and associated lymph nodes[52] from ulcerative colitis patients have been previously described. This is the first direct report of the clonal relationships between total small intestinal and circulating IgA^{+}, IgG^{+} and IgM^{+} ASCs and other B cells in donors without gastrointestinal disease. We observed strong clonal relationships between total intestinal and circulating IgA^{+} ASCs. The majority of circulating IgA^{+} ASCs are derived from mucosal immune reactions that occur in the intestine and in lymphoid tissues of the gut and the airway[53]. Most circulating IgA^{+} ASCs detected at steady state are likely homing to the gut, where they proliferate and generate local clones[54]. While our Ab repertoire analysis did not discriminate between B cells entering the intestinal mucosa versus tissue-resident B cells, these findings do support trafficking between the gut and peripheral blood. Although

circulating and intestinal ASCs were highly clonally related, intestinal ASCs displayed distinct phenotypes that may represent imprinting in the intestinal microenvironment.

Dimensionality reduction by PCA revealed novel phenotypic relationships between B cell subsets[17, 18, 29]. In particular we demonstrated that IgM^+ MBCs were phenotypically most related to naïve B cells. The origin of IgM^+ MBCs in humans is controversial as these cells express CD27, can rapidly differentiate to ASCs and exhibit somatic hypermutation in VH genes yet have been detected in the absence of antigen exposure and in patients with genetic defects in CD40-CD40L[55]. Human IgM^+ MBCs have been referred to as natural MBCs due to their ability to be generated *in vitro* by CpG stimulation of transitional B cells[56]. In our analysis, intestinal IgM^+ MBCs were phenotypically related to both naïve B cells and switched MBCs but had a distinct phenotype from any other B cell subset. It is likely that individual subpopulations of IgM^+ MBCs may differ in their origin and requirement for T cell stimulus.

The measurement of multiple markers per individual cell facilitated visualization of the phenotypic relationships between major B cell subsets as has previously been performed for T and B cells[19–22]. In 3D PCA we determined that $CD27^-$ MBCs occupied a transitional phenotypic niche between IgM^+ MBCs and switched MBCs. $CD27^-$ MBCs produce Abs against encountered antigens such as tetanus toxoid and influenza but not against pneumococcal polysaccharides[57]. $CD27^-$ IgA^+ MBCs in circulation have limited proliferation potential and are present in CD40L-deficient patients, reflecting a GC independent origin. In contrast $CD27^-IgG^+$ MBCs are likely derived from GC reactions[58]. In our analysis most intestinal $CD27^-$ MBCs were IgA^+, a subset associated with innate effector functions[58] and T-independent responses. Within the ASC, switched MBC, and $CD27^-$ MBC subsets, distinct phenotypic clusters were identified in PCA based on isotype expression. IgG^+ ASCs were phenotypically more distinct from IgA^+ ASCs and IgM^+ ASCs. Since intestinal and circulating IgA^+ ASC were clonally related, the distinct phenotypes of IgG^+ ASC may reflect distinct regulation of IgG^+ plasma cell differentiation[36]. Further studies will be required to investigate the functional implications of these observations of the phenotypic relationships between B cell subsets revealed in this analysis.

In conclusion, we used mass cytometry to provide a high dimensional view of the phenotypic heterogeneity of total and VP6-specific intestinal and circulating B cells. We establish the use of metal-tagged proteins for high dimensional analysis of antigen-specific B cells. This work broadens our understanding of the regulation of humoral memory at mucosal surfaces at steady state and lays the foundation for understanding perturbations induced by disease. These data may also aid in the design of improved next generation mucosal vaccines.

METHODS

Human subjects

Proximal jejunum tissue resections were obtained from adults undergoing bariatric surgery at the Stanford Hospital for weight reduction. Informed consent was obtained to collect

peripheral blood (40 ml) intra-operatively. Leukocyte reduction system chambers containing PBMCs from aphaeresis donors were obtained from the Stanford Blood Center. This study was performed in accordance with Stanford University IRB protocols.

Isolation of B cells from jejunum tissue and peripheral blood

Jejujum tissue resections were processed within 1–2 h of surgery. Viable mononuclear cells representative of the lymphoid population present in the gastrointestinal mucosa were isolated as described[59] with modification. Tissue fragments were digested for 1 h at 37 °C with Liberase TL (Roche) (0.26 Wünsch Units/ml). Intestinal and circulating B cells were enriched using EasySep Human B cell Enrichment Kit without CD43 Depletion and RosetteSep Human B cell Enrichment Cocktail (Stemcell Technologies, Vancouver, Canada), respectively, according to manufacturer's instructions. Isolated B cells were incubated at 37 °C in 5% CO_2 for 2 h prior to staining. Cell surface markers that were expressed at comparable levels with and without liberase treatment were included in the analysis.

Antibody labeling

Unconjugated antibodies (carrier protein-free) listed in Table S1 were labeled with heavy metal-loaded maleimide-coupled MaxPar chelating polymers (DVS Sciences, Sunnyvale, CA) according to manufacturer's instructions. Independent comparisons of DN3 and X8 polymers by the manufacturer show minimal differences and thus DN3 polymers were used to be consistent with previous experiments. Metal-labeled Abs were titrated and tested to ensure staining patterns were consistent with those previously reported by flow cytometry as described[19].

RRV DLP preparation and labeling

RRV was grown in MA104 cells in the presence of trypsin as described[60]. RRV triple-layered particles (TLPs) were purified from MA104 cell lysates by genetron extraction, centrifugation through a sucrose cushion, and cesium chloride (CsCl) density gradient centrifugation as described[61, 62]. DLPs were generated by treating TLPs with 20 nM EDTA to remove VP4 and VP7. Purified DLPs were dialyzed to remove residual CsCl. DLPs (100 μg) were labeled with Er166-loaded maleimide-coupled DN3 MaxPar chelating polymer (DVS Sciences) according to manufacturer's instructions.

Mass cytometry staining and data acquisition

B cells were stained for mass cytometry analysis as described[19, 20] with the Abs listed in Table S1. Data were acquired on the CyTOF instrument (DVS Sciences) with noise-reduction mode turned off. For VP6-specific B cell staining, 2 μg of DLP-Er166 was used to stain 2–3 million B cells for 45 min on ice prior to staining with the metal-tagged antibody cocktail. The concentration of DLP-Er166 used for staining was determined in titration experiments on VP6- and VP4-specific hybridomas (not shown).

Mass cytometry data analysis

Mass cytometry data were analyzed using FlowJo (Treestar, version 9.4) using FCS files generated by cell identifying software[19]. For SPADE analysis, clustering was performed using Cytobank (DVS Sciences) [24] based on the expression of B cell lineage markers among all donors analyzed. For PCA, total circulating and intestinal B cells were split into ASC versus non-ASC groups, exported as FCS files, and imported into R using the flowCore R package[63]. Each experiment, consisting of pairs of blood and intestine-derived B cells from the same patient, was analyzed separately. ASC and non-ASC groups were also analyzed separately. To equally weight the blood and intestine-derived cells, an equal number of cells were randomly selected from each sample and used for PCA using the prcomp R function. Scores for each component calculated for each cell were appended to the FCS files and used for subsequent analysis in FlowJo[19]. For 3D plots, a protein data bank formatted file was exported and visualized using PyMol software[64].

Flow cytometry

VP6-specific B cell staining was performed with VLP VP2-eGFP/VP6 (2 μg per test) prior to staining B cells with a fluorescently-tagged Ab panel as described (anti-CD3-PE Cy7 (clone: SKY, Becton Dickinson, San Jose, CA), anti-CD14 PE Cy7 (clone: M5E2, BD), anti-CD16-PE Cy7 (clone: 3G8, BD), anti-CD56-PE Cy7 (clone: B159, BD), anti-CD19 (clone: Sj25C1, BD), anti-CD20-APC H7 (clone: 2H7, BD), anti-CD27-PE (clone: MT271, BD), anti-CD38 (clone: HIT2, BD), anti-IgA (clone: IS11-8E10, Miltenyi Biotec), and anti-IgG (clone: G18-145, BD)) [8, 13]. VLPs VP2-eGFP/VP6 were generated as described[65]. The concentration of VLPs required per staining reaction was determined in titration experiments on VP6- and VP4-specific hybridomas. Data were acquired on the BD FACS Aria III or LSR II with DIVA software version 8.0 (Becton Dickinson). At least 100, 000 events were acquired per sample.

Elispot

The frequencies of total IgA^+ ASCs were determined by Elispot as described[13]. The frequency of intestinal IgA^+ ASCs was determined prior to and following sorting of ASCs and MBCs with and without 1000 U/ml IL-2 (R&D Systems, Minneapolis, MN) and 2.5 μg/ml CpG-2006 (Invivogen, San Diego, CA) for 5 days at 37 °C in 5% CO_2. Cells were harvested after 5 days of stimulation, washed three times in complete RPMI, plated and analyzed as described above.

qRT-PCR

Total RNA was isolated from enriched intestinal B cells and sorted intestinal ASCs and MBCs using RNeasy Micro kit (Qiagen, Venlo, Netherlands). Reverse transcription was performed with Oligo dT using the Affinity Script QPCR cDNA Synthesis kit (Agilent, Santa Clara, CA). Real-time quantitative PCR (qPCR) for human *B-2 microglobulin*, *Bcl-2, Bcl-6*, *Blimp-1*, *IRF-4*, and *XBP-1* transcripts was performed using Taqman gene expression assays (Applied Biosystems, Foster City, CA). Three independent PCRs were performed in triplicate, and results were analyzed using the comparative method with normalization of the

expression of each transcript to 1 in the pre-sorted enriched B cell fraction. qPCRs with threshold cycle (Ct) >35 were not considered significant.

Immune Repertoire Sequencing

Total RNA (500 ng) was used for library preparation. Reverse transcription was performed using primers for isotypes containing 8 random nt and partial Illumina adapters containing barcodes. Second-strand synthesis was performed using primers containing 8 random nt and partial Illumina adapter sequences covering all V segments with a maximum of one mismatch. cDNA was purified and amplified and sequencing libraries were generated by purifying the PCR product. Data was analyzed as described with IGH lineages defined by 90% nucleotide identity between CDR3s[30].

Statistical analysis

Statistical analyses were performed using GraphPad Prism (version 6.0b). Correlations were performed using Pearson's or Spearman's tests. The unpaired t-test was used to compare differences between groups. P values <0.05 were considered significant.

Supplementary Material

Refer to Web version on PubMed Central for supplementary material.

Acknowledgments

The authors would like to thank M. Leipold for CyTOF instrument assistance, N. Sigal for help with reagents, M. Metruccio for advice on qRT-PCR analysis and H. Mei for critical feedback. This work was supported by NIH AI021362, U19 AI090019 (US/India Bilateral Collaborative subaward) and NIH AI057229. N.N. is supported by the Lucile Packard Foundation for Children's Health, NIH-NCATS-CTSA UL1 TR001085 and Child Health Research Institute of Stanford.

References

1. Lanata CF, Fischer-Walker CL, Olascoaga AC, Torres CX, Aryee MJ, Black RE. Global causes of diarrheal disease mortality in children <5 years of age: a systematic review. PLoS One. 2013; 8(9):e72788. [PubMed: 24023773]
2. Brandtzaeg P, Farstad IN, Johansen FE, Morton HC, Norderhaug IN, Yamanaka T. The B-cell system of human mucosae and exocrine glands. Immunol Rev. 1999; 171:45–87. [PubMed: 10582165]
3. Czerkinsky C, Holmgren J. Enteric vaccines for the developing world: a challenge for mucosal immunology. Mucosal Immunol. 2009; 2(4):284–287. [PubMed: 19421181]
4. WHO. Estimated rotavirus deaths for children under 5 years of age: 2008, 453 000. 2012.
5. Feng N, Lawton JA, Gilbert J, Kuklin N, Vo P, Prasad BV, et al. Inhibition of rotavirus replication by a non-neutralizing, rotavirus VP6-specific IgA mAb. J Clin Invest. 2002; 109(9):1203–1213. [PubMed: 11994409]
6. Burns JW, Siadat-Pajouh M, Krishnaney AA, Greenberg HB. Protective effect of rotavirus VP6-specific IgA monoclonal antibodies that lack neutralizing activity. Science. 1996; 272(5258):104–107. [PubMed: 8600516]
7. Vega CG, Bok M, Vlasova AN, Chattha KS, Gomez-Sebastian S, Nunez C, et al. Recombinant monovalent llama-derived antibody fragments (VHH) to rotavirus VP6 protect neonatal gnotobiotic piglets against human rotavirus-induced diarrhea. PLoS Pathog. 2013; 9(5):e1003334. [PubMed: 23658521]

8. Rojas OL, Narvaez CF, Greenberg HB, Angel J, Franco MA. Characterization of rotavirus specific B cells and their relation with serological memory. Virology. 2008; 380(2):234–242. [PubMed: 18789807]

9. Parez N, Garbarg-Chenon A, Fourgeux C, Le Deist F, Servant-Delmas A, Charpilienne A, et al. The VP6 protein of rotavirus interacts with a large fraction of human naïve B cells via surface immunoglobulins. Journal of virology. 2004; 78(22):12489–12496. [PubMed: 15507636]

10. Tian C, Luskin GK, Dischert KM, Higginbotham JN, Shepherd BE, Crowe JE Jr. Immunodominance of the VH1-46 antibody gene segment in the primary repertoire of human rotavirus-specific B cells is reduced in the memory compartment through somatic mutation of nondominant clones. J Immunol. 2008; 180(5):3279–3288. [PubMed: 18292552]

11. Weitkamp JH, Kallewaard NL, Bowen AL, Lafleur BJ, Greenberg HB, Crowe JE Jr. VH1-46 is the dominant immunoglobulin heavy chain gene segment in rotavirus-specific memory B cells expressing the intestinal homing receptor alpha4beta7. J Immunol. 2005; 174(6):3454–3460. [PubMed: 15749880]

12. Weitkamp JH, Kallewaard N, Kusuhara K, Bures E, Williams JV, LaFleur B, et al. Infant and adult human B cell responses to rotavirus share common immunodominant variable gene repertoires. J Immunol. 2003; 171(9):4680–4688. [PubMed: 14568943]

13. Narvaez CF, Feng N, Vasquez C, Sen A, Angel J, Greenberg HB, et al. Human rotavirus-specific IgM Memory B cells have differential cloning efficiencies and switch capacities and play a role in antiviral immunity in vivo. J Virol. 2012; 86(19):10829–10840. [PubMed: 22855480]

14. Di Niro R, Mesin L, Raki M, Zheng NY, Lund-Johansen F, Lundin KE, et al. Rapid generation of rotavirus-specific human monoclonal antibodies from small-intestinal mucosa. J Immunol. 2010; 185(9):5377–5383. [PubMed: 20935207]

15. Bendall SC, Simonds EF, Qiu P, Amir el AD, Krutzik PO, Finck R, et al. Single-cell mass cytometry of differential immune and drug responses across a human hematopoietic continuum. Science. 2011; 332(6030):687–696. [PubMed: 21551058]

16. Ornatsky O, Baranov VI, Bandura DR, Tanner SD, Dick J. Multiple cellular antigen detection by ICP-MS. J Immunol Methods. 2006; 308(1–2):68–76. [PubMed: 16336974]

17. Bagwell CB. Breaking the dimensionality barrier. Methods in molecular biology. 2011; 699:31–51. [PubMed: 21116977]

18. Clark NR, Ma'ayan A. Introduction to statistical methods to analyze large data sets: principal components analysis. Science signaling. 2011; 4(190):tr3. [PubMed: 21917717]

19. Newell EW, Sigal N, Bendall SC, Nolan GP, Davis MM. Cytometry by time-of-flight shows combinatorial cytokine expression and virus-specific cell niches within a continuum of CD8+ T cell phenotypes. Immunity. 2012; 36(1):142–152. [PubMed: 22265676]

20. Newell EW, Sigal N, Nair N, Kidd BA, Greenberg HB, Davis MM. Combinatorial tetramer staining and mass cytometry analysis facilitate T-cell epitope mapping and characterization. Nat Biotechnol. 2013; 31(7):623–629. [PubMed: 23748502]

21. Fergusson JR, Smith KE, Fleming VM, Rajoriya N, Newell EW, Simmons R, et al. CD161 Defines a Transcriptional and Functional Phenotype across Distinct Human T Cell Lineages. Cell reports. 2014; 9(3):1075–1088. [PubMed: 25437561]

22. Bendall SC, Davis KL, Amir el AD, Tadmor MD, Simonds EF, Chen TJ, et al. Single-cell trajectory detection uncovers progression and regulatory coordination in human B cell development. Cell. 2014; 157(3):714–725. [PubMed: 24766814]

23. Benckert J, Schmolka N, Kreschel C, Zoller MJ, Sturm A, Wiedenmann B, et al. The majority of intestinal IgA+ and IgG+ plasmablasts in the human gut are antigen-specific. J Clin Invest. 2011; 121(5):1946–1955. [PubMed: 21490392]

24. Qiu P, Simonds EF, Bendall SC, Gibbs KD Jr, Bruggner RV, Linderman MD, et al. Extracting a cellular hierarchy from high-dimensional cytometry data with SPADE. Nat Biotechnol. 2011; 29(10):886–891. [PubMed: 21964415]

25. Horowitz A, Strauss-Albee DM, Leipold M, Kubo J, Nemat-Gorgani N, Dogan OC, et al. Genetic and environmental determinants of human NK cell diversity revealed by mass cytometry. Sci Transl Med. 2013; 5(208):208ra145.

26. Klein U, Dalla-Favera R. Germinal centres: role in B-cell physiology and malignancy. Nat Rev Immunol. 2008; 8(1):22–33. [PubMed: 18097447]
27. Yoshida T, Mei H, Dorner T, Hiepe F, Radbruch A, Fillatreau S, et al. Memory B and memory plasma cells. Immunol Rev. 2010; 237(1):117–139. [PubMed: 20727033]
28. Medina F, Segundo C, Rodriguez C, Brieva JA. Regulatory role of CD95 ligation on human B cells induced in vivo capable of spontaneous and high-rate Ig secretion. Eur J Immunol. 1997; 27(3): 700–706. [PubMed: 9079812]
29. Genser B, Cooper PJ, Yazdanbakhsh M, Barreto ML, Rodrigues LC. A guide to modern statistical analysis of immunological data. BMC Immunol. 2007; 8:27. [PubMed: 17963513]
30. Vollmers C, Sit RV, Weinstein JA, Dekker CL, Quake SR. Genetic measurement of memory B-cell recall using antibody repertoire sequencing. Proc Natl Acad Sci U S A. 2013; 110(33):13463–13468. [PubMed: 23898164]
31. Farstad IN, Norstein J, Brandtzaeg P. Phenotypes of B and T cells in human intestinal and mesenteric lymph. Gastroenterology. 1997; 112(1):163–173. [PubMed: 8978355]
32. Farstad IN, Carlsen H, Morton HC, Brandtzaeg P. Immunoglobulin A cell distribution in the human small intestine: phenotypic and functional characteristics. Immunology. 2000; 101(3):354–363. [PubMed: 11106939]
33. Farstad IN, Halstensen TS, Lazarovits AI, Norstein J, Fausa O, Brandtzaeg P. Human intestinal B-cell blasts and plasma cells express the mucosal homing receptor integrin alpha 4 beta 7. Scand J Immunol. 1995; 42(6):662–672. [PubMed: 8552990]
34. Medina F, Segundo C, Campos-Caro A, Salcedo I, Garcia-Poley A, Brieva JA. Isolation, maturational level, and functional capacity of human colon lamina propria plasma cells. Gut. 2003; 52(3):383–389. [PubMed: 12584220]
35. Shaw RD, Groene WS, Mackow ER, Merchant AA, Cheng EH. VP4-specific intestinal antibody response to rotavirus in a murine model of heterotypic infection. J Virol. 1991; 65(6):3052–3059. [PubMed: 1709695]
36. Pinto D, Montani E, Bolli M, Garavaglia G, Sallusto F, Lanzavecchia A, et al. A functional BCR in human IgA and IgM plasma cells. Blood. 2013; 121(20):4110–4114. [PubMed: 23550036]
37. Fritz JH, Rojas OL, Simard N, McCarthy DD, Hapfelmeier S, Rubino S, et al. Acquisition of a multifunctional IgA+ plasma cell phenotype in the gut. Nature. 2012; 481(7380):199–203. [PubMed: 22158124]
38. Wang TT, Palese P. Universal epitopes of influenza virus hemagglutinins? Nat Struct Mol Biol. 2009; 16(3):233–234. [PubMed: 19234464]
39. Amanna IJ, Slifka MK. Quantitation of rare memory B cell populations by two independent and complementary approaches. J Immunol Methods. 2006; 317(1–2):175–185. [PubMed: 17055526]
40. Kallewaard NL, McKinney BA, Gu Y, Chen A, Prasad BV, Crowe JE Jr. Functional maturation of the human antibody response to rotavirus. J Immunol. 2008; 180(6):3980–3989. [PubMed: 18322207]
41. Bouvet JP, Fischetti VA. Diversity of antibody-mediated immunity at the mucosal barrier. Infect Immun. 1999; 67(6):2687–2691. [PubMed: 10338470]
42. Monteiro RC. The role of IgA and IgA Fc receptors as anti-inflammatory agents. J Clin Immunol. 2010; 30 (Suppl 1):S61–64. [PubMed: 20405182]
43. Slifka MK, Ahmed R. Long-lived plasma cells: a mechanism for maintaining persistent antibody production. Curr Opin Immunol. 1998; 10(3):252–258. [PubMed: 9638360]
44. Mesin L, Di Niro R, Thompson KM, Lundin KE, Sollid LM. Long-lived plasma cells from human small intestine biopsies secrete immunoglobulins for many weeks in vitro. J Immunol. 2011; 187(6):2867–2874. [PubMed: 21841131]
45. Cassese G, Arce S, Hauser AE, Lehnert K, Moewes B, Mostarac M, et al. Plasma cell survival is mediated by synergistic effects of cytokines and adhesion-dependent signals. J Immunol. 2003; 171(4):1684–1690. [PubMed: 12902466]
46. Hauser AE, Debes GF, Arce S, Cassese G, Hamann A, Radbruch A, et al. Chemotactic responsiveness toward ligands for CXCR3 and CXCR4 is regulated on plasma blasts during the time course of a memory immune response. J Immunol. 2002; 169(3):1277–1282. [PubMed: 12133949]

47. Hiepe F, Radbruch A. Is long-term humoral immunity in the mucosa provided by long-lived plasma cells? A question still open. Eur J Immunol. 2006; 36(5):1068–1069. [PubMed: 16639706]
48. Peperzak V, Vikstrom I, Walker J, Glaser SP, LePage M, Coquery CM, et al. Mcl-1 is essential for the survival of plasma cells. Nat Immunol. 2013; 14(3):290–297. [PubMed: 23377201]
49. Crotty S, Johnston RJ, Schoenberger SP. Effectors and memories: Bcl-6 and Blimp-1 in T and B lymphocyte differentiation. Nat Immunol. 2010; 11(2):114–120. [PubMed: 20084069]
50. Kunkel EJ, Butcher EC. Plasma-cell homing. Nat Rev Immunol. 2003; 3(10):822–829. [PubMed: 14523388]
51. Thoree VC, Golby SJ, Boursier L, Hackett M, Dunn-Walters DK, Sanderson JD, et al. Related IgA1 and IgG producing cells in blood and diseased mucosa in ulcerative colitis. Gut. 2002; 51(1): 44–50. [PubMed: 12077090]
52. Tabibian-Keissar H, Zuckerman NS, Barak M, Dunn-Walters DK, Steiman-Shimony A, Chowers Y, et al. B-cell clonal diversification and gut-lymph node trafficking in ulcerative colitis revealed using lineage tree analysis. Eur J Immunol. 2008; 38(9):2600–2609. [PubMed: 18792412]
53. Mei HE, Yoshida T, Sime W, Hiepe F, Thiele K, Manz RA, et al. Blood-borne human plasma cells in steady state are derived from mucosal immune responses. Blood. 2009; 113(11):2461–2469. [PubMed: 18987362]
54. Yuvaraj S, Dijkstra G, Burgerhof JG, Dammers PM, Stoel M, Visser A, et al. Evidence for local expansion of IgA plasma cell precursors in human ileum. J Immunol. 2009; 183(8):4871–4878. [PubMed: 19786537]
55. Reynaud CA, Descatoire M, Dogan I, Huetz F, Weller S, Weill JC. IgM memory B cells: a mouse/human paradox. Cell Mol Life Sci. 2012; 69(10):1625–1634. [PubMed: 22481437]
56. Capolunghi F, Rosado MM, Sinibaldi M, Aranburu A, Carsetti R. Why do we need IgM memory B cells? Immunology letters. 2013; 152(2):114–120. [PubMed: 23660557]
57. Wirths S, Lanzavecchia A. ABCB1 transporter discriminates human resting naïve B cells from cycling transitional and memory B cells. Eur J Immunol. 2005; 35(12):3433–3441. [PubMed: 16259010]
58. Berkowska MA, Driessen GJ, Bikos V, Grosserichter-Wagener C, Stamatopoulos K, Cerutti A, et al. Human memory B cells originate from three distinct germinal center-dependent and -independent maturation pathways. Blood. 2011; 118(8):2150–2158. [PubMed: 21690558]
59. Fiocchi C, Youngman KR. Isolation of human intestinal mucosal mononuclear cells. Curr Protoc Immunol. 2001; Chapter 7(Unit 7):30. [PubMed: 18432842]
60. Cuadras MA, Feigelstock DA, An S, Greenberg HB. Gene expression pattern in Caco-2 cells following rotavirus infection. J Virol. 2002; 76(9):4467–4482. [PubMed: 11932413]
61. Bridger JC, Woode GN. Characterization of two particle types of calf rotavirus. J Gen Virol. 1976; 31(2):245–250. [PubMed: 180243]
62. Cohen J. Ribonucleic acid polymerase activity associated with purified calf rotavirus. J Gen Virol. 1977; 36(3):395–402. [PubMed: 21225]
63. Ellis, BPH.; Hahne, F.; Le Meur, N.; Gopalakrishnan, N. R package version 1263. flowCore: Basic structures for flow cytometry data. R package version 1.26.3.
64. DeLano, WL. The PyMol Molecular Graphics System. 2002.
65. Charpilienne A, Nejmeddine M, Berois M, Parez N, Neumann E, Hewat E, et al. Individual rotavirus-like particles containing 120 molecules of fluorescent protein are visible in living cells. J Biol Chem. 2001; 276(31):29361–29367. [PubMed: 11356839]

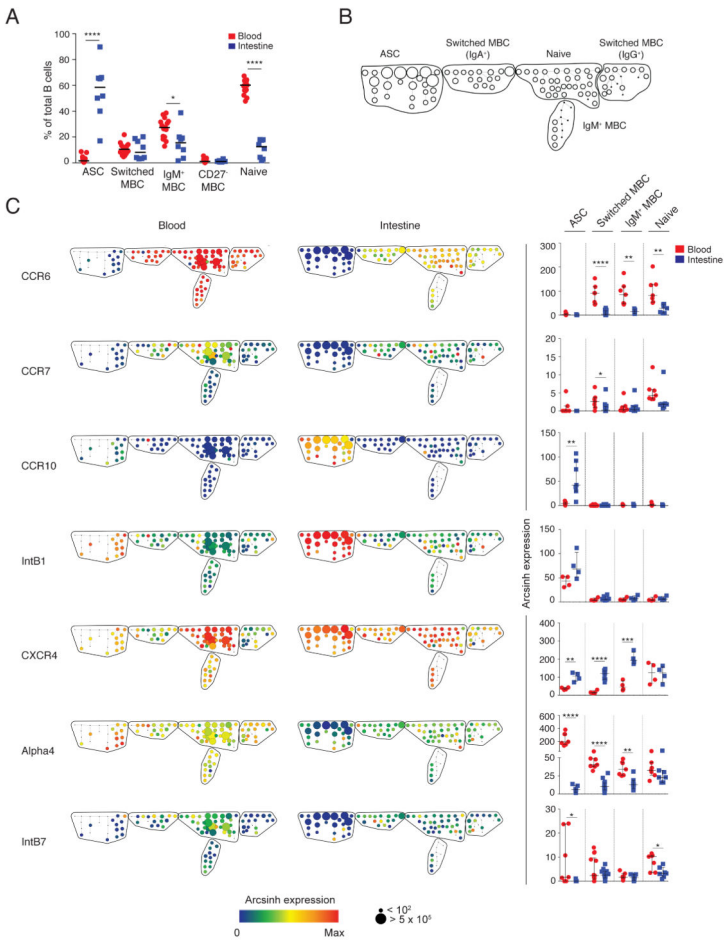

Figure 1. Heterogeneity of mucosal trafficking marker expression in ASCs and other B cell subsets in the intestine and blood at steady state

(A) The median proportions of each B cell subset relative to total intestinal and circulating B cells is shown for eighteen donors. **(B)** B cell subsets were identified based on the expression of lineage markers. Shown is the skeleton structure of the SPADE tree for circulating and intestinal B cells based on data from seven donors. **(C)** Representative SPADE trees (left) depict the expression of markers in the blood and intestine of a single donor. Node color represents arcsinh expression of marker indicated, and node size represents frequency, as indicated in the scale below the tree. Dot plots (right) represent the median arcsinh expression ± range of each marker across B cell subsets in the intestine and blood for the seven donors. * P<0.05; ** P<0.005; *** P<0.0005; **** P<0.00005; unpaired t-test.

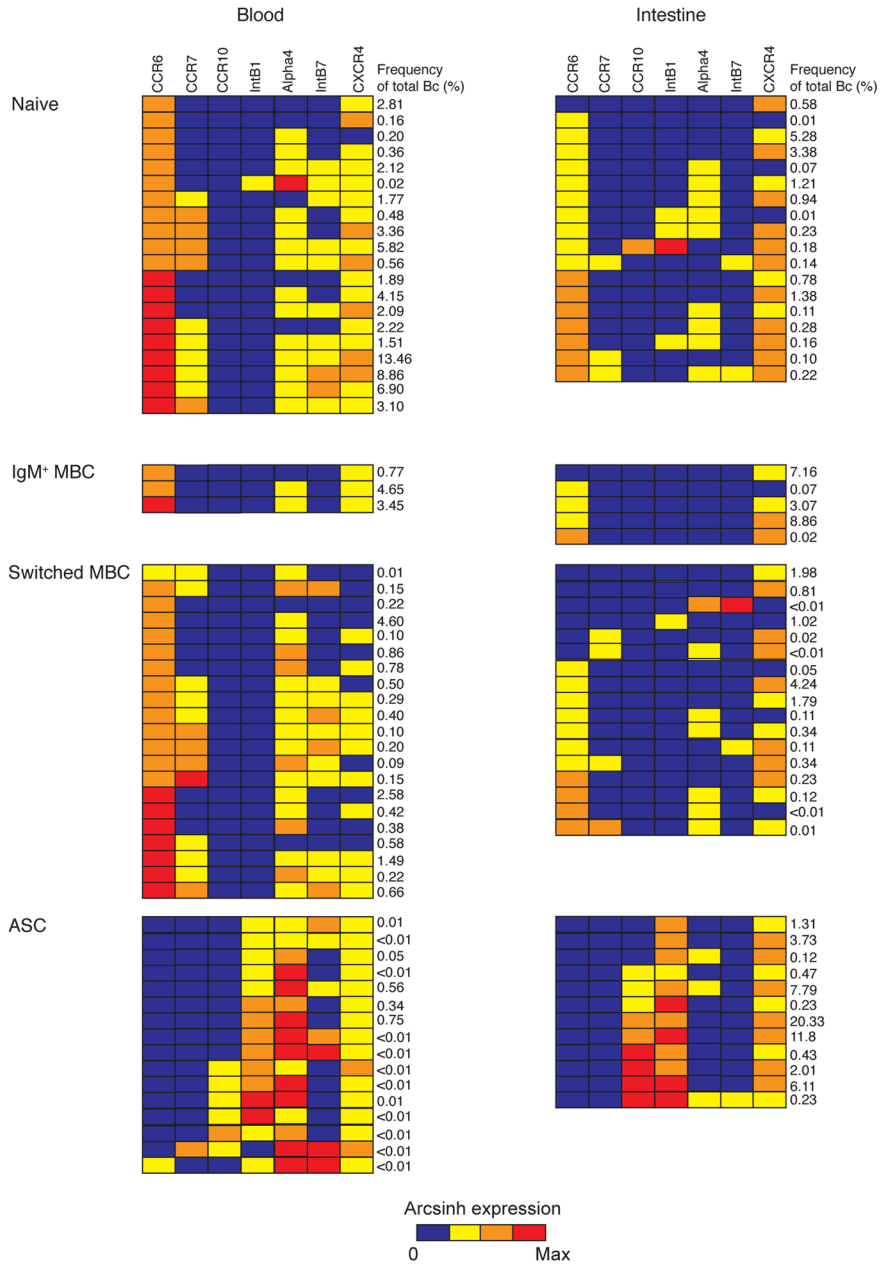

Figure 2. Combinatorial expression of mucosal trafficking markers in ASCs and other B cell subsets in the intestine and blood at steady state

(A) The median arcsinh expression of CCR6, CCR7, CCR10, IntB1, CXCR4, Alpha4 and IntB7 in each individual node of the SPADE tree shown in Fig. 1 was determined in seven donors analyzed. Shown are the cumulative patterns of expression of those markers in each node in the intestine and the blood of seven donors analyzed. Each row represents a distinct mucosal trafficking phenotype. The frequency of each phenotype as a proportion of total intestinal or circulating B cells is indicated on the right. Block color represents arcsinh expression of marker indicated on top according to the 4-point color scale below the graph. Phenotypes are grouped into their respective annotated B cell subsets indicated on the left.

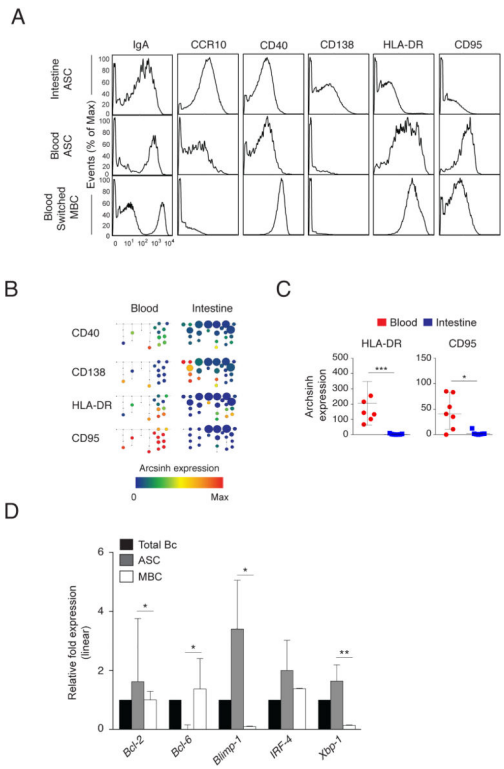

Figure 3. Intestinal ASCs exhibit phenotypic and transcriptional characteristics of long-lived plasma cells

(A) Representative mass cytometry histograms demonstrating differential expression of surface markers in intestinal and circulating ASCs and in circulating switched MBCs of the same donor. **(B)** Marker expression in peripheral blood and intestinal ASC nodes of the SPADE tree shown in Fig. 2 from a representative donor. **(C)** Median arcsinh expression ± range of HLA-DR and CD95 in ASCs in the blood and intestine of seven donors. * P<0.05; *** P<0.0005; unpaired t-test. **(D)** Median relative expression ± range of *Bcl-2, Bcl-6*, *Blimp-1*, *IRF-4*, and *XBP-1* mRNAs in total intestinal B cells and sorted intestinal ASCs and MBCs from three donors. * P<0.05; ** P<0.005; unpaired t-test.

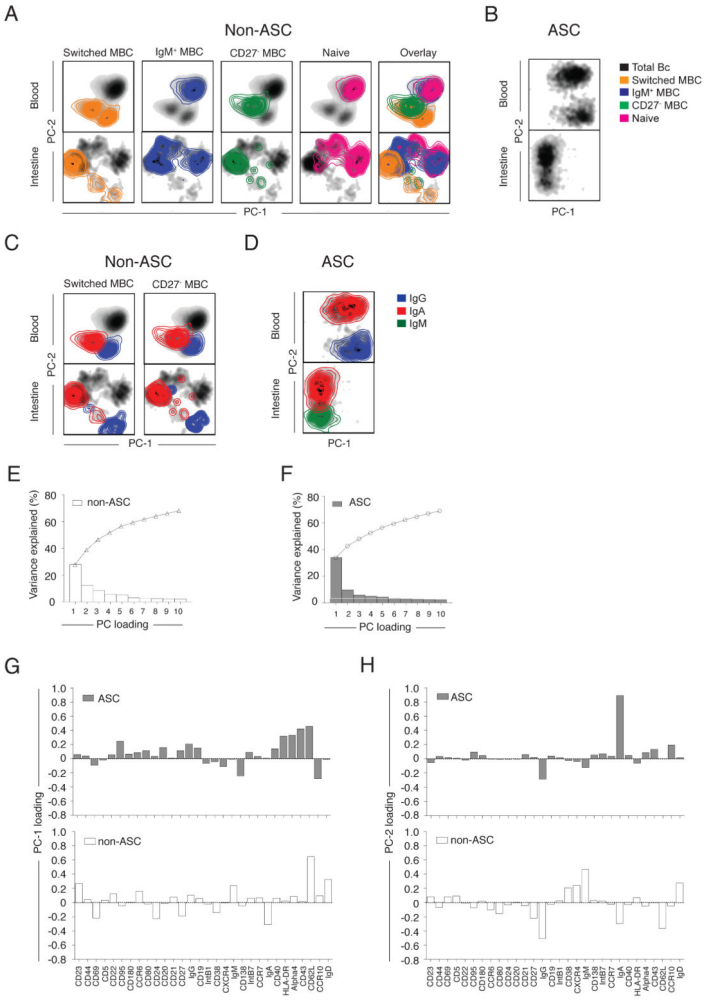

Figure 4. Dimensionality reduction by PCA reveals phenotypic relationships among ASCs and non-ASC B cell subsets

Colored density plots of the first two principal components representing **(A)** gated non-ASC B cell subsets and **(B)** ASCs from the blood and intestine of a representative donor. Colored contour plots of the first two principal components representing the **(C)** IgG^+ and IgA^+, subsets within switched MBCs and $CD27^-$ MBCs and **(D)** IgG^+, IgA^+ and IgM^+ subsets within ASCs in the peripheral blood and intestine of the same representative donor. Percent variation for each component (bars) and cumulatively (line) for **(E)** non-ASCs and **(F)** ASCs. Principal component loading values for the **(G)** PC-1 and **(H)** PC-2 for ASCs and non-ASCs for each parameter.

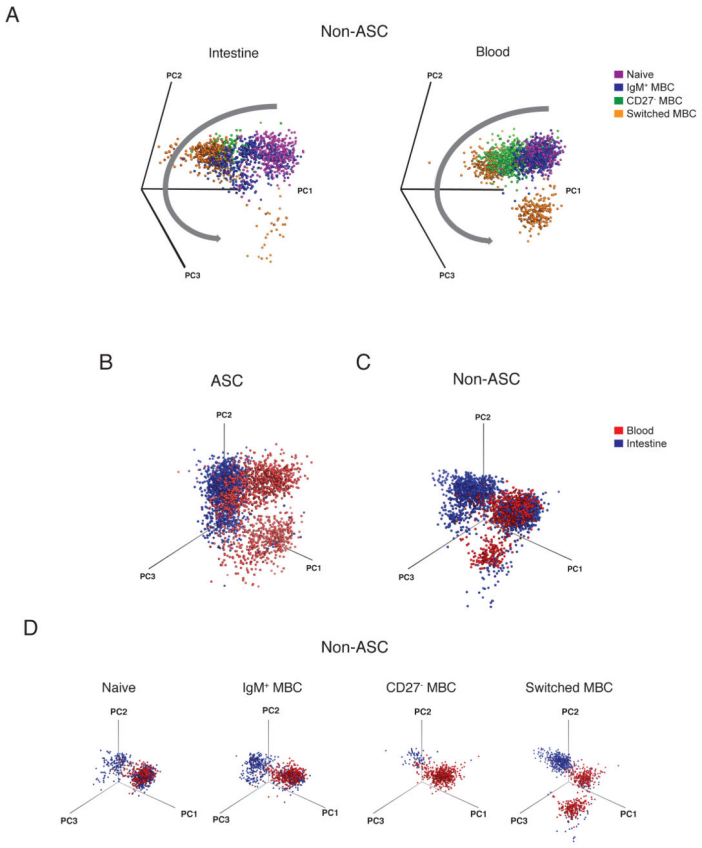

Figure 5. Divergent trajectories of B cell development in the intestine and blood

(A) Visualization of the first three principal components using Pymol reveals phenotypic relationships between major B cell subsets in the intestine and blood. Shown are major non-ASC subsets from a representative donor. Gray arrow indicates the direction of progressive differentiation. 3D visualizations of the phenotypic niches occupied by **(B)** ASCs and **(C)** non-ASCs. **(D)** 3D visualizations of non-ASCs further resolved into naïve B cells, IgM^+ MBCs, $CD27^-$ MBCs and switched MBCs in the intestine and blood of the same donor. Data are represented from the same donor shown in Fig. 4.

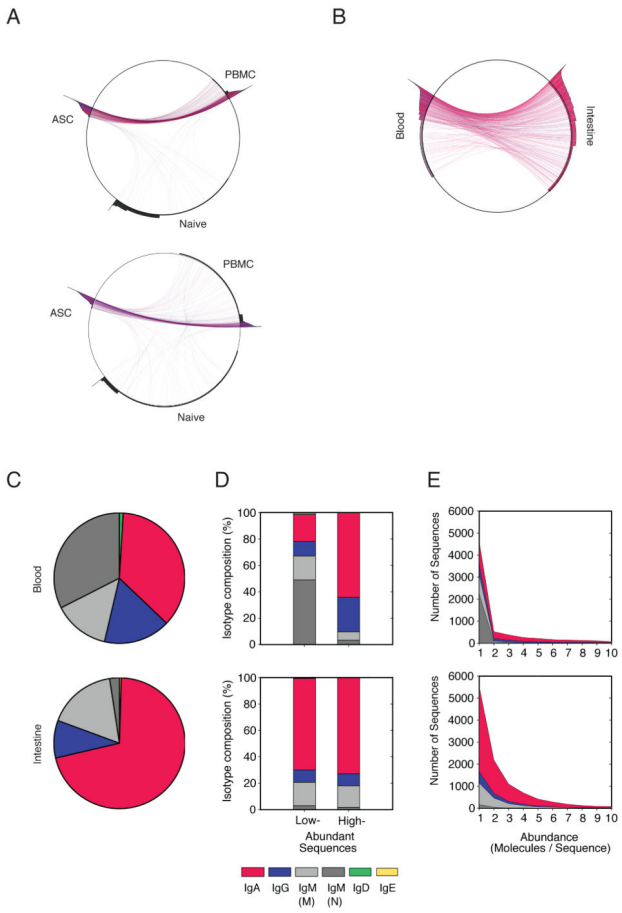

Figure 6. Total intestinal and circulating ASCs are highly clonally related

(A) Identification of total ASC and naïve B cell Ab lineages among total PBMCs. Peripheral blood ASCs and naïve B cells were sorted to ≥98% purity. For two donors, lineages in each cell fraction are plotted on circumference of the circle. Area outside the circle represents the abundance of the respective lineages (logarithmic). Lineages present in two fractions are connected with lines colored according to their isotype (IgA, red; IgG, blue; IgM, black). **(B)** Visualization of lineages shared between total B cells in the intestine and the blood of the same donor. Samples were subsampled to equivalent sequencing depth to facilitate quantitative comparisons. **(C)** Isotype distribution of all Ig sequences analyzed from total circulating and intestinal B cells obtained from the same donor. **(D, E)** Isotype distribution in the same donor represented according to sequence abundance.

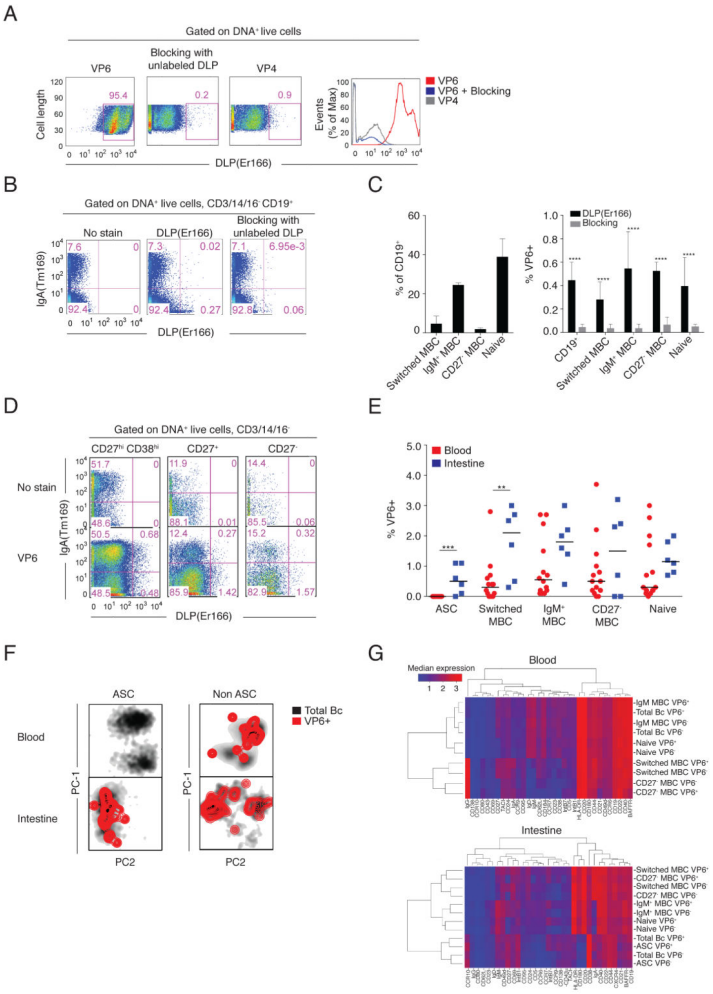

Figure 7. Intestinal and circulating ASCs and other B cell subsets demonstrate VP6 reactivity at steady-state in healthy immune donors

(A) DLP-Er166 stained VP6- but not VP4-specific hybridomas. Blocking with unlabeled DLPs reduced VP6-specific staining on VP6-specific hybridomas. Shown are 2D mass cytometry plots and histogram overlay. **(B)** DLP-Er166 stained human peripheral blood B cell subsets reported to have VP6-reactivity. Staining was blocked with unlabeled DLPs. Shown are representative 2D mass cytometry plots of data from a single donor. **(C)** Bar graph of median frequencies ± range of switched MBCs, IgM^+ MBCs, $CD27^-$ MBCs and naïve B cells among $CD19^+$ cells, and of VP6-binding B cells in subsets, with and without pre-incubation with unlabeled DLPs, as determined by mass cytometry in samples from two donors. **** P<0.00005, unpaired t-test. **(D)** DLP-Er166 stained human intestinal B cell subsets. Shown are representative 2D mass cytometry dot plots from a single donor. **(E)** The median proportions of VP6-specific B cells relative to total B cell subsets in the blood and the intestine of seven donors, as determined by mass cytometry. ** P<0.005; *** P<0.0005; unpaired t-test. **(F)** PCA reveals the distribution of VP6-binding B cells among total ASCs and non-ASCs in the blood and intestine of a representative donor (same donor used in Fig. 4). **(G)** Clustered heatmaps show the median expression of markers among VP6-specific and

VP6-non-specific B cells within B cell subsets in the blood and intestine of a representative donor.